ACS APPLIED MATERIALS & INTERFACES

www.acsami.org

Research Article

Transparent Metallized Microfibers as Recyclable Electrostatic Air Filters with Ionization

Min-Woo Kim,[‖] Seongpil An,*[,‖] Hyunjun Seok, Alexander L. Yarin,* and Sam S. Yoon*

Cite This: https://dx.doi.org/10.1021/acsami.0c01697

Read Online

ACCESS | Metrics & More | Article Recommendations | Supporting Information

ABSTRACT: Air-quality control remains a major environmental concern as polluted air is a threat to public safety and health in major industrialized cities. To filter pollutants, fibrous filters employing electrostatic attraction have been widely used. However, such air filters suffer from some major disadvantages, including low recyclability and a significant pressure drop owing to clogging and a high packing density. Herein, we developed ionization-assisted electrostatic air filters consisting of nonwoven nanofibers. Ionization of particulate matter (PM) using air ionization enhanced the electrostatic attraction, thereby promoting efficient filtration. Metallization of the fibers facilitated strong electrical attraction and the consequent capture of PM of various sizes. The low packing density of the metallized fibers also facilitated efficient filtration of the PM, even at low driving pressures, which in turn reduced the energy consumption of the air-filtration device.

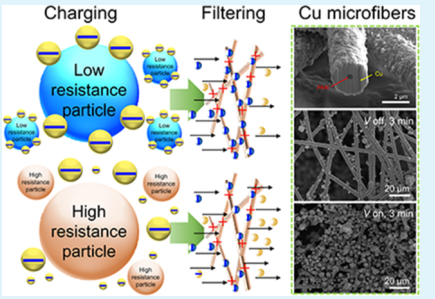

KEYWORDS: *electrospinning, electroplating, metallized nanofibers, electrostatic air filtration, ionizer-assisted filtration*

1. INTRODUCTION

Various industrial sectors, including power plants, gasoline-based automobiles, and manufacturing plants, continue to issue large amounts of particulate matter (PM) annually, resulting in severe air pollution.[1−5] Air pollution associated with PM has become a major public safety concern. Polluted air is a health hazard, especially to elders and children, whose respiratory functions are vulnerable to pollution. PM, having a broad range of sizes and morphologies, causes various diseases in humans.[6−8] For these reasons, numerous methods for passively controlling indoor air pollution have been intensely studied.[9]

Electrostatic precipitators (ESPs) have recently gained research interest as a means of resolving the issue of pressure loss during conventional fiber filtration.[10−12] ESPs operate via the following mechanism: gas-borne particles are ionized through air ionization and pass through an electric field. These particles are charged with electrons and thus are electrically negative. The particles are immobilized through electrical attraction induced by a positively charged electrode, which is often grounded.[13] Despite the advancements in ESP technology, one major issue remains unresolved: The ESP filters are often incapable of collecting medium-size PM, which is too small to be collected using ordinary filtration and too large to be collected using electrostatic attraction. In light of this technological challenge, ESPs have been supplemented with wet scrubbers,[14] two-stage electrostatic precipitators,[15] and carbon fiber electrodes as potential solutions.[16] Though remedial, these strategies are not a complete solution to the issues of capturing medium-size PM.

Fiber-based nonwoven air filters account for more than 70% of the entire air-filter market. Nanofiber-based filters may offer high permeability, low weight, and cost-effectiveness. In addition, nanofibers can be decorated with functional materials that can enhance filtration efficiency[17] and capture particular toxic particles such as formaldehyde[18,19] and heavy metal ion.[20] The packing density of such filters can be readily controlled by controlling the fiber size and filter thickness. These fiber-based filters are also energy-efficient as they afford a relatively high permeability while maintaining good filtration efficiency.[21,22] Fiber-based filters can be manufactured using various materials, such as glass,[23] thermoplastics,[24] ceramics,[25] cellulose,[26,27] and metal.[28] Fiber-fabrication methods include meltblowing,[23] island in the sea spinning,[29] self-assembly,[30] templating,[31,32] and electrospinning,[33,34] among which the latter is particularly useful for producing very fine fibers that can be easily modified via metal-plating and decoration with functional materials.[34−36]

Within this framework, a combined approach utilizing the electrostatic attraction of ESP and fiber-based filters has been introduced for efficient PM capture.[37−44] Air ionization and charging of PMs can increase the electrostatic attraction of the particles and thus increase filtration efficiency while circumventing the issue of pressure loss.[45] However, even this hybrid

Received: January 28, 2020
Accepted: May 6, 2020

system (combining nanofibers and ESP features) may still suffer from the issues of pressure loss after clogging and poor recyclability when the fiber packing density is high. If the packing density of the filter is increased to capture a relatively small PM, the operating pressure (and hence the energy consumption) must increase to compensate for the pressure loss associated with the increased packing density. Once the fibrous filter is clogged, its recycling is nearly impossible and impractical; low filter recyclability is an issue that needs to be addressed to improve the environmental friendliness of the filters. Thus, more reliable, efficient, environmentally friendly, industrially viable, and cost-effective approaches must be developed.

Herein, we introduce nanofibers electroplated with metal, resulting in significantly enhanced electrostatic attraction, even with low packing densities. The metallized fiber filters developed in the present study can improve the overall conductivity of the resulting filters due to the presence of the metallic shell surrounding the electrospun polymer nanofiber core. Furthermore, PM is ionized in ionized air to further enhance the electrostatic attraction between the precharged PM and the metallized fibrous filters. The effects of fiber metallization, PM size, and PM material type are investigated. On the other hand, in general, as the velocity of airflow during filtration increases, not only does the filtration efficiency decrease but the pressure drop should increase accordingly.[43,46] However, the metallized fiber filters developed in the present study exhibit high filtration efficiency and low pressure drop even under the conditions of the high-velocity airflow.

The packing density and recyclability of the metallized fibrous filter are also compared with those of commercial filters (i.e., air-purifier filters and vacuum-cleaner filters) to elucidate the novelty and benefits of the proposed filtration method.

Figure 1 illustrates the difference between the filtration mechanisms of electrically low-resistance particles and high-

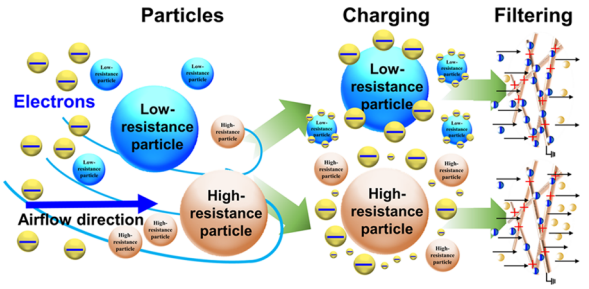

Figure 1. Effect of electrical resistance of PM on ionization features.

resistance particles. For example, metal (Cu or Ni) particles are low-resistance materials, while plastic or metal-oxide (TiO_2) particles are high-resistance materials. When these particles are subjected to the same level of the surrounding air ionization, the low-resistance particles are charged with a greater number of electrons, while the high-resistance particles are charged with considerably fewer electrons. Air ionization may occur when electrons are discharged from the pin, resulting in ionization of the surrounding air.[13,47] The electrons released from air molecules in the avalanche-like ionization process attach to the PM and confer a negative charge to the particles.[47,48] These negatively charged particles are electrically attracted and adhere to the grounded metallized fibers, as shown in Figure 1. Accordingly, electrons are conducted to the ground through the metallized fibers, causing the metallized fibers to maintain their electrical neutrality and continue to attract the PM.[49]

2. EXPERIMENTAL SECTION

2.1. PAN Nanofibers and Cu Microfibers. Figure 2 shows the process used for fabricating copper (Cu) microfibers via the

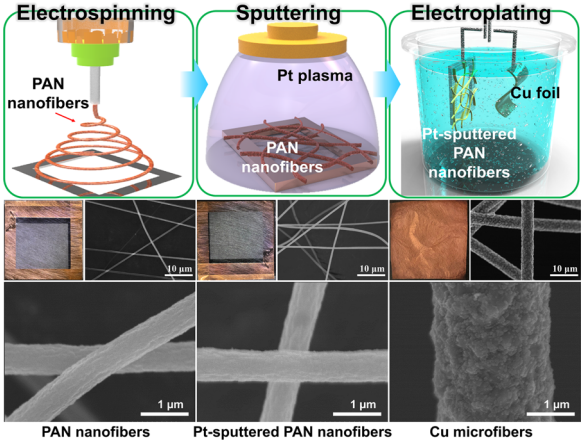

Figure 2. Schematic of the process used for fabricating Cu microfiber filters: (left) electrospinning, (middle) sputtering, and (right) electroplating. The snapshots and scanning electron microscopy (SEM) images below the panels correspond to the fibers resulting from each process.

combined electrospinning and electroplating techniques.[33,50−62] First, an electrospinning solution comprising 8 wt % polyacrylonitrile (PAN, $(C_3H_3N)_n$, M_w = 150 kDa, Sigma-Aldrich) and *N*,*N*-dimethyl formamide (DMF, 99.8%, Sigma-Aldrich) was prepared by dissolving PAN in DMF and then magnetically stirring the mixed solution at room temperature (20 °C) for 24 h. Thereafter, the fully dissolved 8 wt % PAN solution was electrospun using a syringe pump (Legato 100, KDS) and a DC power supply (EL20P2, Glassman High Voltage Inc.). The electrospinning parameters are listed in Table 1. Note that

Table 1. Details of the Fabrication Processes Based on Electrospinning and Electroplating

process	parameters	values
electrospinning	applied DC voltage (kV)	6
	flow rate (μL/h)	280
	nozzle-to-collector distance (cm)	13
	electrospinning time (s)	180 (PAN nanofiber filter)
		60 (Cu microfiber filter)
electroplating	applied voltage (kV)	3
	fiber mat-to-Cu electrode distance (cm)	3
	electroplating time (s)	60

two types of PAN nanofibers were employed in the present study. The PAN nanofibers with the electrospinning time of 180 s were used for PAN nanofiber filters (cf. Section 3), while the PAN nanofibers with the electrospinning time of 60 s were used for the production of Cu microfiber filters as follows.

The Cu microfibers were obtained by electroplating the electrospun PAN nanofibers (formed with the electrospinning time of 60 s) with a Cu electroplating solution (Figure 2). The solution for Cu electroplating was prepared by mixing 80 g of copper sulfate ($CuSO_4$,

https://dx.doi.org/10.1021/acsami.0c01697
ACS Appl. Mater. Interfaces XXXX, XXX, XXX−XXX

Sigma-Aldrich), 25 g of sulfuric acid (H_2SO_4, Matsunoen Chemicals), 2.5 g of hydrochloric acid (HCl, Sigma-Aldrich), 50 g of formaldehyde (CH_2O, Sigma-Aldrich), and 500 mL of distilled (DI) water. Prior to the Cu electroplating process, sputtering was used to seed platinum (Pt) on the electrospun PAN nanofibers to initiate electroplating on the metal nuclei (seeds) provided by sputtering. The Pt seeds had diameters of 10 nm or less.

For Cu electroplating, a DC power supply (E3664A, Agilent Technologies) and a homemade electroplating setup were used under the operating conditions detailed in Table 1. Here, it should be noted that the electroplating time was chosen as 60 s based on the results previously reported by this group,[33] where the Cu microfibers Cu-plated for 60 s revealed the highest performance in the PM removal. In addition, in the case of the Cu microfibers formed with electroplating time below 30 s, even though the PM removal performance was insignificantly different from that after 60 s Cu plating, the mechanical durability was lower (after 30 s than after 60 s).

After electroplating, the electroplated Cu microfibers were rinsed with DI water and then immediately dried with nitrogen gas to prevent oxidation. As demonstrated in Figure 2, sputtering did not alter the thickness of the nanofibers because the sputtered Pt was of the scale of a few nanometers. Electroplating thickened the nanofibers significantly with the diameter of the resulting fibers being in the 2−3 μm range.

2.2. Characterization. The fiber morphology was characterized using high-resolution scanning electron microscopy (HR-SEM, Philips Co., the Netherlands) at an operating power of 15 kV. For the comparison of the packing densities of different fibers, the area ratios of fibers were measured from multiple SEM images (three SEM images for each case) using I-measure software, where the area ratio of fibers was calculated by dividing the two-dimensional (2D) area of the fibers in the SEM image by the total area of the SEM image. In detail, an SEM image was converted to a black and white image, in which the white and black areas corresponded to the fibers and the empty space, respectively. The white area was divided by the total area and multiplied by 100%, which defined the value of the area ratio (cf. Figure S1). An average value from three SEM images for each case is mentioned in the present study.

To obtain the cross-section SEM image of a Cu microfiber, focused ion beam (FIB, Quanta 3D FEG, FEI Company) was used, where the Cu microfiber was cut with gallium ions by the FIB milling process that was conducted with a beam current of 7 nA at 30 kV.

The weight of the PM collected before and after filtration was measured using an electronic scale (PAG214C, Ohaus) with a high precision (±0.0001 g) at 20 °C by measuring the weight difference between the PM-captured and bare Cu microfiber filter. The transmittance of each filter was measured using a ultraviolet−visible (UV−vis) spectrophotometer (Optizen POP, Mecasys, Daejeon, Korea). The transmittance was measured in the 400−1100 nm wavelength range based on air transmittance (T = 100%).

Tensile and out-of-plane stress tests were performed for both the Cu microfiber and PAN nanofiber mats using a homemade testing device, in which a force gauge (FG-6020SD, Lutron Electronic) was installed and a syringe pump (Legato 100, KD Scientific Inc.) was used to create a constant stretching speed of a specimen. The size of the tested mats was 2.0 cm × 2.5 cm, and the stretching speed was 0.05 mm/s. To further characterize the mechanical-bending properties of the mats, an automatic bending tester (COAD.722, Ocean Science, Republic of Korea) was used with the bending speed being set to 20 mm.

2.3. Air Ionizer. To precharge the PM negatively, high-frequency alternating current (AC) air ionization was employed.[63−65] A high-frequency air ionizer (Zapp II, Shishido Electrostatic, Ltd., Japan) moved toward the powder (or PM) feeder precharging the PM in contact with ionized air. In the experiments, a total of five different powders was used as PM: Cu powder 1 [~625 mesh, APS (Aerodynamic Particle sizer) 0.50−1.5 μm, 99% (metal basis), Alfa Aesar], Cu powder 2 [~625 mesh, APS 3.25−4.75 μm, 99.9% (metal basis), Alfa Aesar], Cu powder 3 [spherical, APS 10 μm, 99.9%, Alfa Aesar], titanium dioxide (TiO_2) powder (1500 nm, rutile, 99.9%, Alfa Aesar), and nickel (Ni) powder [APS 2.2−3.0 μm 99.9% (metal basis), C typically <0.25%, Alfa Aesar].

2.4. Filtration Test. Figure 3a illustrates PM precharging inside the PM feeder using an electrified pin, which ionizes the surrounding

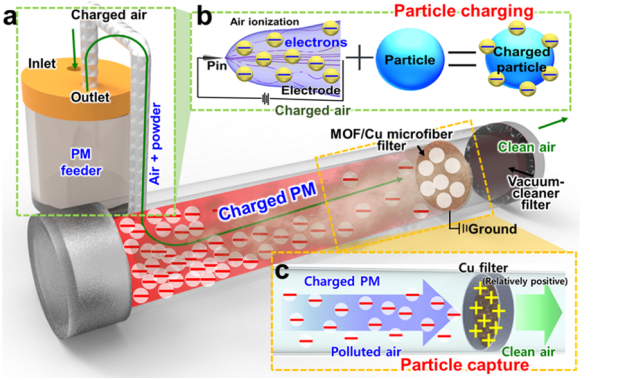

Figure 3. Schematic of the experimental setup for filtration tests. (a) Fluidized PM feeder supplied with charged/ionized air. (b) PM in ionized air resulting in charged PM. (c) Charged PM attracted toward grounded Cu microfiber filter.

air. The precharged PM is fed into the cylinder and filtered through the Cu microfiber filter, which is grounded, thereby attracting the precharged PM. Once PM is attached to the Cu filter, its negative charge is lost to the ground through the Cu fibers (Figure 3b). Air passing through the Cu microfiber filter is thus cleaner and free of PM. The PM passing through the Cu microfiber filter is collected at the vacuum-cleaner filter attached to the end of the cylinder.

The powder feeder was supplied with compressed air, which was used to generate high pressure required to drive the entire flow. The PM species in the powder feeder were fluidized by the injected compressed air and supplied to the cylinder equipped with a Cu microfiber filter and a vacuum-cleaner filter. The compressed air was ionized by an electrified pin prior to being injected into the power feeder. The PM was exposed to the ionized air, and thus negatively charged by electrons released from the avalanche-like ionization process in air. The Cu microfiber filter was grounded and was thus able to attract the precharged PM.

The total mass of the supplied PM is M_0, which comprises the amount of PM collected at the Cu microfiber filter (M_f) and the amount collected at the vacuum-cleaner filter at the cylinder end (M_v): $M_0 = M_f + M_v$. The values of M_0, M_f, and M_v were measured independently, and the above-mentioned balance was fulfilled with the accuracy of 2−3%. The mass of the PM (M_v) collected at the vacuum-cleaner filter at the end of the cylinder was found by measuring the before-and-after weights. The commercial filters used were a vacuum-cleaner filter (VPF-600, Talent filter, Republic of Korea) and an air-cleaner filter (CFX-B100D, BKC Co., Ltd., Republic of Korea).

3. RESULTS AND DISCUSSION

3.1. Cu Microfibers, PM Type, and Size. Figure 4a presents a comparison between the morphologies of the PAN nanofibers and the corresponding electroplated Cu microfibers. The PAN nanofibers were densely packed because the electrospinning time of 180 s was used (cf. Section 2.1). Here, it should be emphasized that different electrospinning times were used to form the PAN nanofibers and the Cu microfibers to make the packing density of the PAN nanofibers similar to that of the Cu microfibers (cf. Section 2.1 and Table 1). This is related to the fact that the use of electroplating onto the electrospun polymer nanofibers caused an increase in the

https://dx.doi.org/10.1021/acsami.0c01697
ACS Appl. Mater. Interfaces XXXX, XXX, XXX−XXX

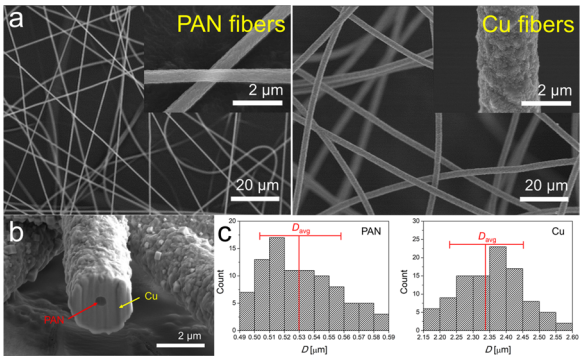

Figure 4. SEM images of (a) PAN nanofibers (left) and Cu microfibers (right). (b) SEM image of the cross section of a Cu microfiber. (c) Size distributions of the PAN nanofibers (left) and Cu microfibers (right).

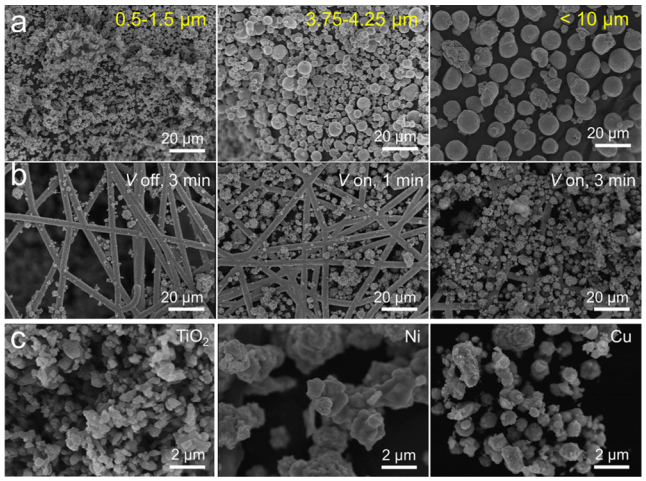

Figure 5. SEM images of (a) Cu PM of various size ranges. (b) Filtered Cu PM on Cu microfibers without and with precharging (1–3 min filtration time). (c) PM of various types: TiO_2, Ni, and Cu.

packing density of fibers due to an overall increase in the fiber diameters. That is, contrary to the electrospinning time for the PAN nanofibers (180 s), the Cu microfibers were produced with the electrospinning time of 60 s.

On the other hand, the area ratio of fibers is proportional to the porosity (or packing density) of the corresponding fiber mats.[33,57,66] To explore the porosity (or packing density) of the PAN nanofiber mats and the Cu microfiber mats, we compared their area ratios by analyzing the SEM images. The area ratios of the PAN nanofibers and Cu microfibers were 31.4% and 34.1%, respectively, which were confirmed by measuring the area occupied in the 2D images by the fibers using the I-measure software. Three different samples for each case were used for this area-ratio measurement, and the values were averaged. It should also be mentioned that the area ratio of the samples was kept constant to ensure a fair comparison between the filtration efficiencies of the filters comprising the PAN nanofibers and Cu microfibers.

Figure 4b shows the SEM image of the cross section of the Cu microfiber, in which it is confirmed that the PAN nanofiber was located at the core, while Cu encased the PAN nanofiber with a constant thickness layer of 1.1 μm. Figure 4c shows the size distributions of the PAN nanofibers and Cu microfibers. Note that the size distribution of each case was established by measuring the corresponding 100 fibers observed in three SEM images. The values of the average diameter (D_{avg}) of PAN nanofibers and Cu microfibers were 0.53 ± 0.03 and 2.34 ± 0.11 μm, respectively. Since the electrospinning time of PAN nanofibers was longer than that for the Cu microfibers, the space between the PAN nanofibers was smaller than that between the Cu microfibers. That is, the PAN nanofibers exhibited a pore size of ~1.7 μm, whereas that of the Cu microfibers was ~7 μm.

Figure 5a presents a comparison of the copper PM of various sizes from 0.5 to 10 μm. The individual size ranges are noted in yellow in each SEM image. For parametric studies, the representative equivalent diameters of D_{Cu} = 1, 4, and 10 μm were selected for the various sizes.

Figure 5b compares the effects of precharging on the PM filtration by the Cu-plated filter. The size range of the PM used herein was 0.5–1.5 μm with the average size being D_{Cu} = 1 μm. When the precharging was turned off, only a small amount of PM was present on the Cu microfibers, even after 3 min of active particle supply through the cylinder. When the precharging was turned on, the PM was effectively collected on the Cu microfibers, and it completely filled the spaces between the fibers for flow times of 1 and 3 min. This comparison confirms the effectiveness of precharging, which produces PM that is strongly attracted to the grounded Cu microfiber filter.

Figure 5c presents SEM images of the TiO_2, Ni, and Cu PM used in this study. TiO_2 PM is a high-electrical resistance material, whereas the other two metal (Ni and Cu) PM species are considered low-resistance materials, which are easily chargeable. The Ni and TiO_2 PM species comprised the largest and smallest particles, respectively. Note that the Cu PM in Figure 5c is the same as that shown in the left image in Figure 5c.

Figure 6 presents images of the filters of various thicknesses. The thickness of the Cu filter was 25 μm, which is sufficiently thin to be transparent. The transparency of this filter is illustrated in the inset in Figure 6a, where letters placed behind the filter are clearly visible because the filter is sufficiently transparent. The thicknesses of the commercial filters (the vacuum cleaner and air purifier) shown in Figure 6b,c were measured using a digital electronic caliper; the measured values were 130 and 590 μm, respectively, which are too high for these filters to be transparent. The thickness of the Cu filter shown in Figure 6d was estimated from the SEM image, which revealed that the greatest thickness of the filter was approximately 25 μm. Certainly, the commercial filters are substantially thicker, and therefore, their packing density is considerably greater, which would require greater pressure to drive airflow across the filters (the area ratios of the vacuum-cleaner and the air-purifier filters were 72.1 and 67.2%, respectively; cf. Figure S1). In contrast, the 25-μm-thick Cu microfiber filter had a relatively low packing density (and thus, transparent) and, accordingly, would require a relatively low pressure to drive the same airflow (the area ratio of the Cu microfiber mats was 34.1%). Clearly, the low packing density of the Cu microfiber filter would permit a greater amount of PM to pass through the filter and thus would result in ineffective filtration if no electrical attraction were induced. However, with electrical attraction, the Cu microfiber filter is capable of capturing precharged PM efficiently despite its low packing density. Figure 6e shows the transmittance of the filters: the transmittance of the Cu microfiber filter was

https://dx.doi.org/10.1021/acsami.0c01697
ACS Appl. Mater. Interfaces XXXX, XXX, XXX–XXX

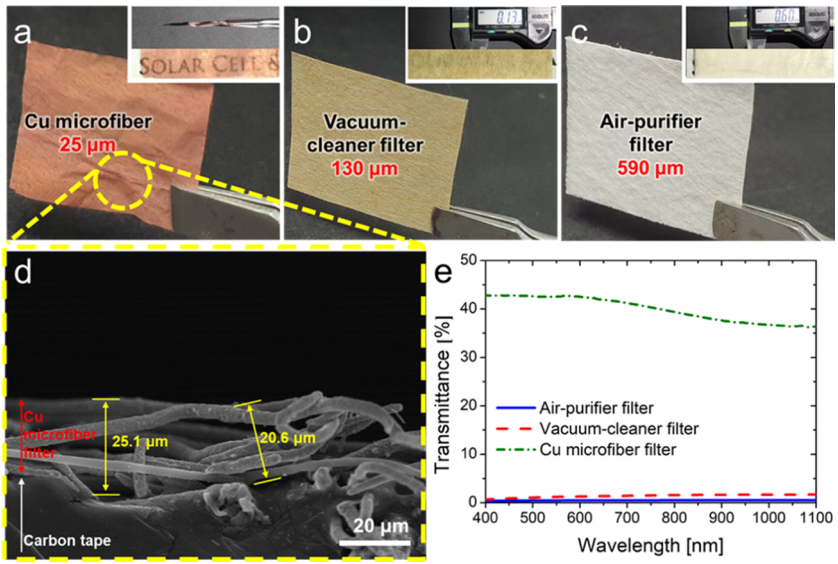

Figure 6. Comparison of filter thickness: (a) Cu microfiber filter (25 μm), (b) vacuum-cleaner filter (130 μm), (c) air-purifier filter (590 μm), (d) SEM image of the cross section of Cu microfiber filter, and (e) transmittance of various filters.

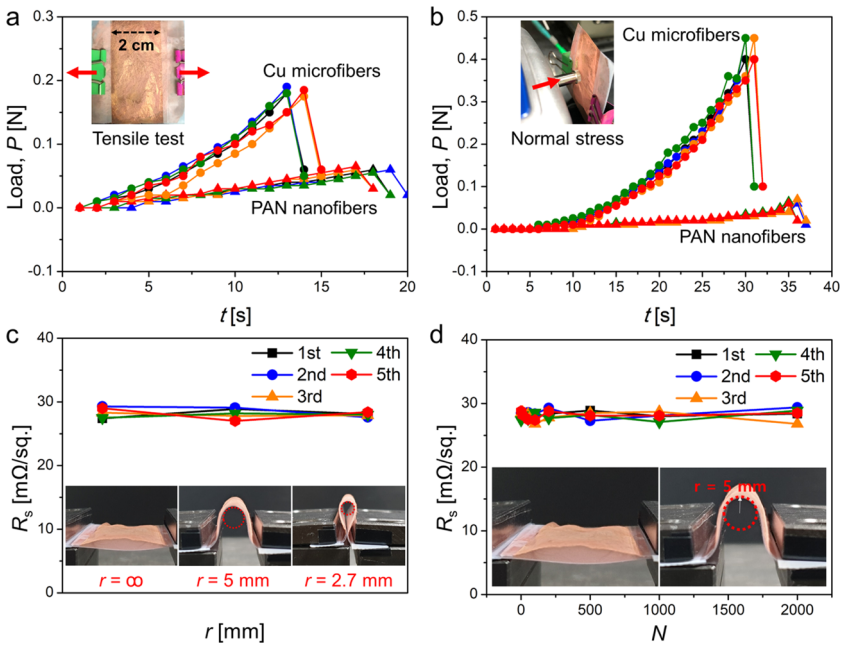

Figure 7. Mechanical and electrical properties of the Cu microfiber filter. Comparison of (a) tensile and (b) bending strength of Cu microfiber and PAN nanofiber filters (both samples have the same cross-sectional porosity). Change in sheet resistance, R_s, with variation in (c) bending radius, r, and (d) the number of bending cycles, N.

approximately 40%, whereas that of the other two commercial filters was 0%.

3.2. Mechanical Properties of the Cu Microfiber Filter.

Figure 7a presents a comparison between the tensile behavior of the Cu microfibers and PAN nanofibers. As previously mentioned in relation to Figure 4a, the porosities of both filters are kept the same to fairly reflect the effect of only the material type (i.e., polymer and copper-plated polymer) and that no other factors (such as the size or packing density) would affect this comparison. Five replicate tests were conducted with five distinctive specimens produced under the same fabrication conditions. The excellent repeatability confirms the accuracy of the results. The PAN (polymer) nanofibers underwent deformation under the applied force and eventually failed with the peak load of 0.065 N at $t \approx 18$ s. The Cu microfibers underwent a similar deformation process and eventually failed with a peak load of 0.19 N at $t \approx 13$ s. The Cu microfibers were definitively stiffer than the PAN nanofibers with the elastic deformation of the former being characterized by a greater slope of the load (P) vs time t curve.

The stiffness of the Cu microfiber filter is also evident from Figure 7b, which presents a comparison in the bending test. The specimen was attached to a paper substrate with a hole in the middle. A stiff rod was pushed in the middle of the specimen until failure. The rod pushing speed was set to 0.05 mm. The Cu microfiber filter failed at a peak strength of 0.45 N, while the PAN nanofiber filter failed at a peak strength of 0.06 N. Five replicate experiments were performed, and the

https://dx.doi.org/10.1021/acsami.0c01697
ACS Appl. Mater. Interfaces XXXX, XXX, XXX−XXX

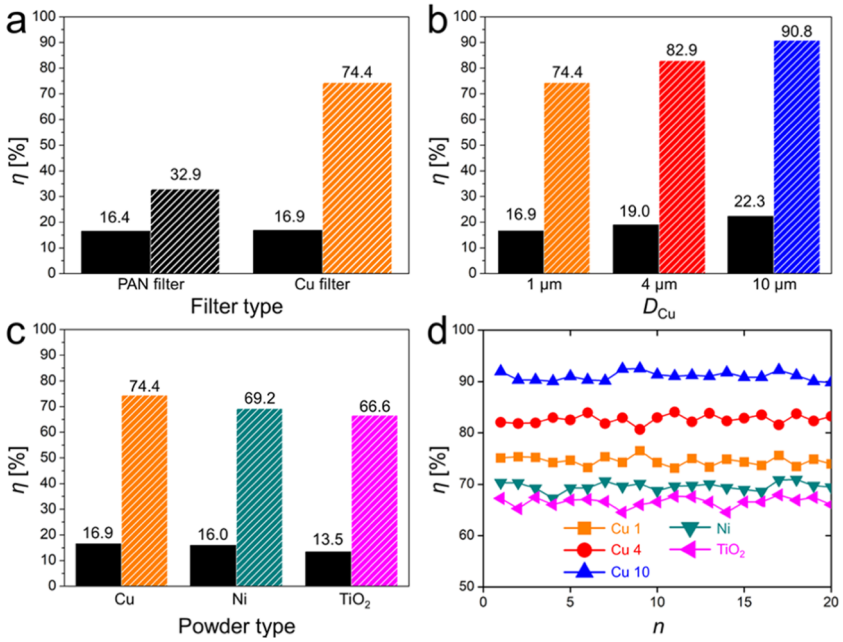

Figure 8. Filtration efficiency of various filters. (a) Effect of the filter type: PAN nanofibers vs Cu microfiber filters. (b) Effect of the size of Cu PM: D_{Cu} = 1, 4, and 10 μm. (c) Effect of PM type (Cu, Ni, and TiO_2). (d) Filter recyclability with Cu, Ni, and TiO_2 PM. Note that the solid black bars denote the cases without precharging, while the shaded bars denote the cases with precharging.

consistent results for both the Cu microfiber filters and PAN nanofiber filters confirm the reliability of the results. Figures 7a and 7b confirm the mechanical superiority of the Cu microfiber filter compared to that of the PAN polymer filter, which is attributed to the presence of the Cu shell.

Figure 7c,d shows the electrical sheet resistance (R_s) of the Cu microfiber filter when the bending radius and the number of bending cycles (up to N = 2000), respectively, were varied. The sheet resistance remained essentially constant even under the severe bending, wherein the radius of curvature was reduced to r = 2.7 mm. At the bending radius of r = 5 mm, the bending cycle was repeated up to N = 2000 with no deterioration in the electrical properties of the Cu microfiber filter being observed, thereby demonstrating the mechanical superiority of such a filter.

3.3. Filtration Efficiency. Figure 8 presents the filtration efficiency, η, of various filters for filtration of the different PM species. The following definition of η is used

$$\eta = \frac{M_f}{M_0} \times 100\% = \left(1 - \frac{M_v}{M_0}\right) \times 100\% \quad (1)$$

Figure 8a compares η for the PAN and Cu microfiber filters for filtration of air containing Cu PM with D_{Cu} = 1 μm. The left black bars represent the cases without precharging and the right shaded bars represent the cases with precharging. There was no difference in the values of η for the PAN and Cu microfiber filters without precharging, with η being 16.4 and 16.9%, respectively. This slight difference in the values of η confirms that the PAN and Cu microfiber filters have practically the same packing density or porosity (the area ratio from Figure 4a) despite differences in the fiber thickness. However, when precharging was applied, the Cu microfiber filter strongly attracted the Cu PM, increasing the filtration efficiency up to η = 74.4%. This confirms the significant influence of PM precharging and the electrical attraction to the grounded filter, as opposed to the PAN (polymer) filter, for which the precharging effect is relatively minor. The precharging effect was, indeed, present even in the case of PAN, resulting in an increased filtration efficiency from η = 16.4 to 32.9%. However, the effect was much smaller than when the Cu microfiber filter was used.

Figure 8b shows the effect of the PM size (D_{Cu}) on the filtration efficiency η. Without precharging, the filtration efficiency was low, but the effect of D_{Cu} was discernible. When D_{Cu} was large, η was higher, indicating that larger PM is easier to collect. This trend also persisted with precharging, but the filtration efficiency η was significantly larger. Therefore, the precharging is the dominant factor that impacts the overall value of η. The precharging effect was sufficiently strong to attract the particles with a size of D_{Cu} = 10 μm. Without the precharging, nearly 78% of the PM with D_{Cu} = 10 μm passed through the Cu microfiber filter without any electrical interference. However, 68.5% more PM was electrically captured by the Cu microfiber filter with precharging, which reveals that precharging was the main driving force for filtration. The filtration efficiencies with small Cu particles (having diameters below 1 μm) were also explored, where the sizes of the Cu particles used were 0.3 and 0.5 μm. The corresponding efficiencies were lower than that for the 1 μm particles. Specifically, the filtration efficiencies for the D_{Cu} = 0.3 and 0.5 μm cases with using the ionizer were 62.6 and 68.2%, respectively (cf. Figure S2a). That is, when the D_{Cu} was below 1 μm, the smaller the particle size was, the lower the filtration efficiency became. This tendency was similar to those previously reported.[67,68] Figure S2 shows the results of the additional filtration experiments with using smaller Cu particles (less than 1 μm in diameter) and varying the flow rate. The corresponding pressure drop was also measured at different flow rates. Figure S2a shows the filtration efficiency of Cu particles with sizes less than 1 μm. As the particle size decreased from 1 to 0.5 and 0.3 μm, the corresponding filtration efficiencies decreased from 74.4 to 68.2 and 62.6%

https://dx.doi.org/10.1021/acsami.0c01697
ACS Appl. Mater. Interfaces XXXX, XXX, XXX−XXX

(with the ionizer being turned on). The tendency exhibited here was similar to the results shown in Figure 8b.

Prior to the tests illustrated in Figure 8c, all types of PM (Cu, Ni, and TiO_2) were sieved through a 1.5 μm mesh. Thus, most of the PM had sizes below 1.5 μm. Figure 8c shows the effect of the powder type (i.e., of the particle material) on the filtration efficiency η. Without precharging, there was essentially no difference in the values of η for Cu and Ni metal particles because both were of similar sizes. In the case of TiO_2 PM, η was slightly smaller than those for Cu and Ni PM, probably because of the smaller particle size of TiO_2, which allowed more PM to pass through the filter. This minor effect of the PM size induced a 2−3% variation in η. With precharging, the filtration efficiency was in the $66 \leq \eta \leq 75\%$ range. Cu and Ni PM are both highly conducting, and therefore, η did not differ significantly for these species, although the 5.2% difference may be attributed to the higher conductivity of Cu relative to that of Ni. TiO_2 PM was also considerably affected by precharging, even though TiO_2 is a dielectric material having low electrical conductivity (see Table 2). The slightly lower value of η for TiO_2 PM relative to those of Cu and Ni indicates that the powder type (or the electrical conductivity of the material) does have an effect on the overall filtration efficiency η because the inherent nature of the PM determines the extent to which it can be precharged. However, these differences appear to be relatively small (less than 8% in the values of η), while the influence of precharging itself is considerably higher (larger than 50% in the values of η).

Table 2. Electrical Resistivity of Cu, Ni, and TiO_2

materials	resistivity (Ω m)
Cu	1.71×10^{-8}
Ni	8.2×10^{-6}
TiO_2	1×10^{11}−1×10^{16}

In addition, we explored the filtration efficiency with varying airflow rates and the corresponding pressure drops. Note that the basic airflow rate was 50 L/min, and the corresponding filtration efficiency with using the ionizer was 74.4%. As the flow rate increased from 50 to 75 and 100 L/min, the filtration efficiency also increased from 74.4 to 81.4 and 88.6%. (cf. Figure S2b). A pressure gauge (DPG 3000, New-Flow Technologies, Inc., accuracy: ±0.5% of full scale) was installed in the experimental setup to observe the pressure drop between the inlet and the outlet of the setup (cf. Figure S2d). There were no discernible pressure drops when the flow rates were 50 and 70 L/min, as revealed in Figure S2d. As the flow rate became 100 L/min, the corresponding pressure drop also slightly increased to 0.01 psi.

Figure 8d illustrates the recyclability of the Cu microfiber filter in the cases with various particle types and sizes. The symbols Cu 1, Cu 4, and Cu 10 refer to the Cu PM with D_{Cu} = 1, 4, and 10 μm, respectively. Each symbol represents the test under airflow for 3 min with precharging. After each 3 min test, the Cu microfiber filter was cleaned using the air blowing technique (for 30 s at a flow rate of 20 mL/min and a nozzle diameter of 7 mm), as illustrated in Figure 9. Figure 9a presents snapshots of the Cu microfiber filter before and after each test with subsequent cleaning for up to n = 20 cycles (only the n = 1 and 20 cases are presented for brevity). The SEM images in Figure 9b show the Cu microfiber filter before and after cleaning by air blowing. This comparison confirms the effectiveness of the air-blowing cleaning technique. Although some PM still remained on the Cu microfiber surface, most of the PM was detached from the fibers, and the open areas were visibly clean, which would permit further filtration. The data in Figure 8d confirm that the filtration efficiency remained essentially constant for all cycles, irrespective of the particle type and size. This excellent repeatability indicates that the Cu microfiber filter can be used essentially indefinitely, as long as the physical structure of the electroplated copper on the fibers remains intact. Similarly, the effects of electroplating, precharging, and air-blowing cleaning for commercial filters were also explored (Figures S3 and S4), where the combination of electroplating and precharging positive influenched the filtration efficiency while the air-blowing cleanging for the repeatability was impractical.

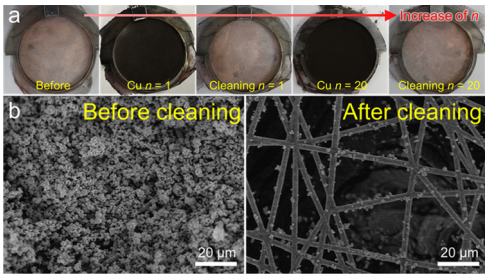

Figure 9. (a) Snapshots of Cu microfiber filter before filtration and after continuous usage for up to n = 20 times with repetitive cleaning after each filtration run. (b) SEM images before and after cleaning. Note that each filtration run lasted up to t = 3 min under airflow with PM.

On the other hand, the measurement of ion concentration or aerosol current is important for designing future ESPs. The charge concentration of particles N (m^{-3}) can be calculated, and using N, an average number of elementary charges collected by the particles n can be also expressed as[66]

$$n = \frac{I}{Q \times N \times e} \quad (2)$$

where I is the electric current in the ESP, Q is the flow rate of air (L/min), and e is the elementary charge (1.6×10^{-19} C). The value of N in the present study is 5.3×10^{11} m^{-3}, which is 1 or 2 orders of magnitude lower than those revealed in the previously reported studies (where the theoretical values of N were 3.5×10^{12} and 2.5×10^{14} m^{-3}, and which had almost similar experimental conditions with those in the present study).[66] This is attributed to the fact that the recombination process continuously occurs while the airflow passes the experimental setup that has a long distance from the ionizer to the filter installed. In other words, there were charge losses due to an electron−ion recombination.[67−69] Note that the value of the measured current and the corresponding charge concentration are listed in Table 3.

Table 3. Charge Concentration Calculated with the Measured Current and Flow Rate

parameter	value
current (C/s)	5.0×10^{-4}
flow rate (L/min)	50
charge concentration (m^{-3})	5.3×10^{11}

https://dx.doi.org/10.1021/acsami.0c01697
ACS Appl. Mater. Interfaces XXXX, XXX, XXX−XXX

4. CONCLUSION

An electrostatic air filter with particulate precharging was fabricated in this study. The filter comprised metallized microfibers that formed a 25-μm-thick mat having a transparency of approximately T = 40%. This metal-plated fiber mat was electrically grounded to create an electric field, attracting negatively charged particulate matter (PM). Air was ionized using an air ionizer, and the ionized air was mixed with the PM in a power feeder prior to injection into the cylinder, which was equipped with a Cu microfiber filter. Upon release of the charged PM into airflow inside the cylinder, the PM was strongly attracted to the Cu microfiber filter, which significantly increased the filtration efficiency (by more than 50%). The effects of the PM type (i.e., of the PM material) and size were also analyzed. Larger PM was more readily filtered as these species were easily captured. Notably, precharging was the dominant factor affecting the filtration efficiency. This dominant effect of precharging was achieved only when the grounded filter was made of metallized microfibers. The metallized filter was recyclable up to 20 times with no deterioration of the filtration performance. Therefore, the precharging-assisted electrostatic air filter with metallized fibers is a potentially viable commercial solution for efficient air cleaning.

■ ASSOCIATED CONTENT

Supporting Information

The Supporting Information is available free of charge at https://pubs.acs.org/doi/10.1021/acsami.0c01697.

SEM images the commercial filter (Figure S1); filtration efficiency of Cu microfiber filters (Figure S2); effect of electroplating on commercial filters (Figure S3); recyclability test for commercial filters (Figure S4) (PDF)

■ AUTHOR INFORMATION

Corresponding Authors

Seongpil An − *SKKU Advanced Institute of Nanotechnology (SAINT) and Department of Nano Engineering, Sungkyunkwan University (SKKU), Suwon 16419, Republic of Korea; Department of Mechanical and Industrial Engineering, University of Illinois at Chicago, Chicago, IIllinois 60607-7022, United States*; Email: esan@skku.edu

Alexander L. Yarin − *Department of Mechanical and Industrial Engineering, University of Illinois at Chicago, Chicago, IIllinois 60607-7022, United States*; orcid.org/0000-0001-8032-2525; Email: ayarin@uic.edu

Sam S. Yoon − *School of Mechanical Engineering, Korea University, Seoul 02841, Republic of Korea*; orcid.org/0000-0002-9031-4198; Email: skyoon@korea.ac.kr

Authors

Min-Woo Kim − *School of Mechanical Engineering, Korea University, Seoul 02841, Republic of Korea; SKKU Advanced Institute of Nanotechnology (SAINT) and Department of Nano Engineering, Sungkyunkwan University (SKKU), Suwon 16419, Republic of Korea*

Hyunjun Seok − *School of Mechanical Engineering, Korea University, Seoul 02841, Republic of Korea*

Complete contact information is available at: https://pubs.acs.org/10.1021/acsami.0c01697

Author Contributions

‖M.-W.K. and S.A. have equally contributed.

Notes

The authors declare no competing financial interest.

■ ACKNOWLEDGMENTS

This research was supported by the Technology Development Program to Solve Climate Changes of the National Research Foundation (NRF) funded by the Ministry of Science, ICT & Future Planning (NRF-2016M1A2A2936760 and NRF-2013R1A5A1073861).

■ REFERENCES

(1) Watson, J. G. Visibility: Science and Regulation. *J. Air Waste Manage. Assoc.* **2002**, *52*, 628−713.

(2) Streets, D. G.; Wu, Y.; Chin, M. Two-Decadal Aerosol Trends as a Likely Explanation of the Global Dimming/Brightening Transition. *Geophys. Res. Lett.* **2006**, *33*, No. L15806.

(3) Andreae, M.; Rosenfeld, D. Aerosol−Cloud−Precipitation Interactions. Part 1. The Nature and Sources of Cloud-Active Aerosols. *Earth-Sci. Rev.* **2008**, *89*, 13−41.

(4) Mahowald, N. Aerosol Indirect Effect on Biogeochemical Cycles and Climate. *Science* **2011**, *334*, 794−796.

(5) Zhang, R.; Jing, J.; Tao, J.; Hsu, S.-C.; Wang, G.; Cao, J.; Lee, C. S. L.; Zhu, L.; Chen, Z.; Zhao, Y.; et al. Chemical Characterization and Source Apportionment of Pm 2.5 in Beijing: Seasonal Perspective. *Atmos. Chem. Phys.* **2013**, *13*, 7053−7074.

(6) Kim, K.-H.; Kabir, E.; Kabir, S. A Review on the Human Health Impact of Airborne Particulate Matter. *Environ. Int.* **2015**, *74*, 136−143.

(7) Brauer, M.; Amann, M.; Burnett, R. T.; Cohen, A.; Dentener, F.; Ezzati, M.; Henderson, S. B.; Krzyzanowski, M.; Martin, R. V.; Van Dingenen, R.; et al. Exposure Assessment for Estimation of the Global Burden of Disease Attributable to Outdoor Air Pollution. *Environ. Sci. Technol.* **2012**, *46*, 652−660.

(8) Hu, J.; Zhang, H.; Chen, S.-H.; Wiedinmyer, C.; Vandenberghe, F.; Ying, Q.; Kleeman, M. J. Predicting Primary Pm2. 5 and Pm0. 1 Trace Composition for Epidemiological Studies in California. *Environ. Sci. Technol.* **2014**, *48*, 4971−4979.

(9) Thakur, R.; Das, D.; Das, A. Electret Air Filters. *Sep. Purif. Rev.* **2013**, *42*, 87−129.

(10) Zuraimi, M.; Tham, K. Reducing Particle Exposures in a Tropical Office Building Using Electrostatic Precipitators. *Build. Environ.* **2009**, *44*, 2475−2485.

(11) Feng, Z.; Long, Z.; Yu, T. Filtration Characteristics of Fibrous Filter Following an Electrostatic Precipitator. *J. Electrost.* **2016**, *83*, 52−62.

(12) Feng, Z.; Long, Z.; Chen, Q. Assessment of Various Cfd Models for Predicting Airflow and Pressure Drop through Pleated Filter System. *Build. Environ.* **2014**, *75*, 132−141.

(13) Parker, K. R. *Applied Electrostatic Precipitation*; Springer: Dordrecht, 1997.

(14) Laitinen, A.; Hautanen, J.; Keskinen, J. Effect of the Space Charge Precipitation on Wet Scrubber Fine Particle Removal Efficiency. *J. Aerosol Sci.* **1997**, *28*, S287−S288.

(15) Gao, M.; Zhu, Y.; Yao, X.; Shi, J.; Shangguan, W. Dust Removal Performance of Two-Stage Electrostatic Precipitators and Its Influencing Factors. *Powder Technol.* **2019**, *348*, 13−23.

(16) Kim, H.-J.; Han, B.; Woo, C. G.; Kim, Y.-J. Ozone Emission and Electrical Characteristics of Ionizers with Different Electrode Materials, Numbers, and Diameters. *IEEE Trans. Ind. Appl.* **2017**, *53*, 459−465.

(17) Zhang, K.; Huo, Q.; Zhou, Y.-Y.; Wang, H.-H.; Li, G.-P.; Wang, Y.-W.; Wang, Y.-Y. Textiles/Metal−Organic Frameworks Composites as Flexible Air Filters for Efficient Particulate Matter Removal. *ACS Appl. Mater. Interfaces* **2019**, *11*, 17368−17374.

(18) Zhao, X.; Chen, L.; Guo, Y.; Ma, X.; Li, Z.; Ying, W.; Peng, X. Porous Cellulose Nanofiber Stringed Hkust-1 Polyhedron Membrane for Air Purification. *Appl. Mater. Today* **2019**, *14*, 96−101.
(19) Zhu, Q.; Tang, X.; Feng, S.; Zhong, Z.; Yao, J.; Yao, Z. Zif-8@ Sio2 Composite Nanofiber Membrane with Bioinspired Spider Web-Like Structure for Efficient Air Pollution Control. *J. Membr. Sci.* **2019**, *581*, 252−261.
(20) Peng, Y.; Huang, H.; Zhang, Y.; Kang, C.; Chen, S.; Song, L.; Liu, D.; Zhong, C. A Versatile Mof-Based Trap for Heavy Metal Ion Capture and Dispersion. *Nat. Commun.* **2018**, *9*, No. 187.
(21) Barhate, R. S.; Ramakrishna, S. Nanofibrous Filtering Media: Filtration Problems and Solutions from Tiny Materials. *J. Membr. Sci.* **2007**, *296*, 1−8.
(22) Payatakes, A. C.; Tien, C. Particle Deposition in Fibrous Media with Dendrite-Like Pattern: A Preliminary Model. *J. Aerosol Sci.* **1976**, *7*, 85−100.
(23) Wang, S.; Zhao, X.; Yin, X.; Yu, J.; Ding, B. Electret Polyvinylidene Fluoride Nanofibers Hybridized by Polytetrafluoroethylene Nanoparticles for High-Efficiency Air Filtration. *ACS Appl. Mater. Interfaces* **2016**, *8*, 23985−23994.
(24) Wang, D.; Sun, G.; Chiou, B. S. A High-Throughput, Controllable, and Environmentally Benign Fabrication Process of Thermoplastic Nanofibers. *Macromol. Mater. Eng.* **2007**, *292*, 407−414.
(25) Sigmund, W.; Yuh, J.; Park, H.; Maneeratana, V.; Pyrgiotakis, G.; Daga, A.; Taylor, J.; Nino, J. C. Processing and Structure Relationships in Electrospinning of Ceramic Fiber Systems. *J. Am. Ceram. Soc.* **2006**, *89*, 395−407.
(26) Kim, C.-W.; Kim, D.-S.; Kang, S.-Y.; Marquez, M.; Joo, Y. L. Structural Studies of Electrospun Cellulose Nanofibers. *Polymer* **2006**, *47*, 5097−5107.
(27) Tursi, A.; De Vietro, N.; Beneduci, A.; Milella, A.; Chidichimo, F.; Fracassi, F.; Chidichimo, G. Low Pressure Plasma Functionalized Cellulose Fiber for the Remediation of Petroleum Hydrocarbons Polluted Water. *J. Hazard. Mater.* **2019**, *373*, 773−782.
(28) Ou, Q.; Maricq, M. M.; Pakko, J.; Chanko, T. B.; Pui, D. Y. Design and Evaluation of a Sintered Metal Fiber Filter for Gasoline Direct Injection Engine Exhaust Aftertreatment. *J. Aerosol Sci.* **2019**, *133*, 12−23.
(29) Zhang, Z.; Tu, W.; Peijs, T.; Bastiaansen, C. W. Fabrication and Properties of Poly (Tetrafluoroethylene) Nanofibres Via Sea-Island Spinning. *Polymer* **2017**, *109*, 321−331.
(30) Qiu, P.; Mao, C. Biomimetic Branched Hollow Fibers Templated by Self-Assembled Fibrous Polyvinylpyrrolidone Structures in Aqueous Solution. *ACS Nano* **2010**, *4*, 1573−1579.
(31) Cao, G.; Liu, D. Template-Based Synthesis of Nanorod, Nanowire, and Nanotube Arrays. *Adv. Colloid Interface Sci.* **2008**, *136*, 45−64.
(32) Tanaka, S.; Doi, A.; Nakatani, N.; Katayama, Y.; Miyake, Y. Synthesis of Ordered Mesoporous Carbon Films, Powders, and Fibers by Direct Triblock-Copolymer-Templating Method Using an Ethanol/Water System. *Carbon* **2009**, *47*, 2688−2698.
(33) Kim, M.-W.; An, S.; Seok, H.; Yoon, S. S.; Yarin, A. L. Electrostatic Transparent Air Filter Membranes Composed of Metallized Microfibers for Particulate Removal. *ACS Appl. Mater. Interfaces* **2019**, *11*, 26323−26332.
(34) Kim, M. H.; Lee, W. J.; Lee, D. H.; Ko, S. W.; Hwang, T. I.; Kim, J. W.; Park, C. H.; Kim, C. S. Development of Nanofiber Reinforced Double Layered Cabin Air Filter Using Novel Upward Mass Production Electrospinning Set Up. *J. Nanosci. Nanotechnol.* **2018**, *18*, 2132−2136.
(35) Ahmed, F. E.; Lalia, B. S.; Hashaikeh, R. A Review on Electrospinning for Membrane Fabrication: Challenges and Applications. *Desalination* **2015**, *356*, 15−30.
(36) Bhardwaj, N.; Kundu, S. C. Electrospinning: A Fascinating Fiber Fabrication Technique. *Biotechnol. Adv.* **2010**, *28*, 325−347.
(37) Agranovski, I. E.; Huang, R.; Pyankov, O. V.; Altman, I. S.; Grinshpun, S. A. Enhancement of the Performance of Low-Efficiency Hvac Filters Due to Continuous Unipolar Ion Emission. *Aerosol Sci. Technol.* **2006**, *40*, 963−968.
(38) Park, J. H.; Yoon, K. Y.; Noh, K. C.; Byeon, J. H.; Hwang, J. Removal of Pm 2.5 Entering through the Ventilation Duct in an Automobile Using a Carbon Fiber Ionizer-Assisted Cabin Air Filter. *J. Aerosol Sci.* **2010**, *41*, 935−943.
(39) Noh, K.-C.; Lee, J.-H.; Kim, C.; Yi, S.; Hwang, J.; Yoon, Y. H. Filtration of Submicron Aerosol Particles Using a Carbon Fiber Ionizer-Assisted Electret Filter. *Aerosol Air Qual. Res.* **2011**, *11*, 811−821.
(40) Park, J. H.; Yoon, K. Y.; Hwang, J. Removal of Submicron Particles Using a Carbon Fiber Ionizer-Assisted Medium Air Filter in a Heating, Ventilation, and Air-Conditioning (Hvac) System. *Build. Environ.* **2011**, *46*, 1699−1708.
(41) Shi, B. Influence of Filter Fiber Material on Removal of Ultrafine and Submicron Particles Using Carbon Fiber Ionizer-Assisted Intermediate Air Filters. *ASHRAE Trans.* **2012**, *118*, 602−611.
(42) Shi, B.; Ekberg, L. Ionizer Assisted Air Filtration for Collection of Submicron and Ultrafine Particles Evaluation of Long-Term Performance and Influencing Factors. *Environ. Sci. Technol.* **2015**, *49*, 6891−6898.
(43) Choi, D. Y.; Jung, S.-H.; Song, D. K.; An, E. J.; Park, D.; Kim, T.-O.; Jung, J. H.; Lee, H. M. Al-Coated Conductive Fibrous Filter with Low Pressure Drop for Efficient Electrostatic Capture of Ultrafine Particulate Pollutants. *ACS Appl. Mater. Interfaces* **2017**, *9*, 16495−16504.
(44) Choi, D. Y.; An, E. J.; Jung, S.-H.; Song, D. K.; Oh, Y. S.; Lee, H. W.; Lee, H. M. Al-Coated Conductive Fiber Filters for High-Efficiency Electrostatic Filtration: Effects of Electrical and Fiber Structural Properties. *Sci. Rep.* **2018**, *8*, No. 5747.
(45) Tian, E.; Mo, J. Toward Energy Saving and High Efficiency through an Optimized Use of a Pet Coarse Filter: The Development of a New Electrostatically Assisted Air Filter. *Energy Build.*. **2019**, *186*, 276−283.
(46) Wake, D.; Brown, R. Measurements of the Filtration Efficiency of Nuisance Dust Respirators against Respirable and Non-Respirable Aerosols. *Ann. Occup. Hyg.* **1988**, *32*, 295−315.
(47) Kelly, E.; Spottiwood, D. The Theory of Electrostatic Separations: A Review Part Ii. Particle Charging. *Miner. Eng.* **1989**, *2*, 193−205.
(48) Kelly, E.; Spottiswood, D. The Theory of Electrostatic Separations: A Review Part Iii. The Separation of Particles. *Miner. Eng.* **1989**, *2*, 337−349.
(49) Barthelemy, R.; Mora, R. In *Electrical High Tension Minerals Beneficiation: Principles and Technical Aspects*, Proceedings of Fifth IMPC; IMM: London, UK, London, UK, 1960; pp 757−773.
(50) An, S.; Lee, C.; Liou, M.; Jo, H. S.; Park, J.-J.; Yarin, A. L.; Yoon, S. S. Supersonically Blown Ultrathin Thorny Devil Nanofibers for Efficient Air Cooling. *ACS Appl. Mater. Interfaces* **2014**, *6*, 13657−13666.
(51) An, S.; Jo, H. S.; Al-Deyab, S. S.; Yarin, A. L.; Yoon, S. S. Nano-Textured Copper Oxide Nanofibers for Efficient Air Cooling. *J. Appl. Phys.* **2016**, *119*, No. 065306.
(52) An, S.; Jo, H. S.; Kim, D. Y.; Lee, H. J.; Ju, B. K.; Al-Deyab, S. S.; Ahn, J. H.; Qin, Y.; Swihart, M. T.; Yarin, A. L.; Yoon, S. S. Self-Junctioned Copper Nanofiber Transparent Flexible Conducting Film Via Electrospinning and Electroplating. *Adv. Mater.* **2016**, *28*, 7149−7154.
(53) An, S.; Kim, Y. I.; Sinha-Ray, S.; Kim, M.-W.; Jo, H. S.; Swihart, M. T.; Yarin, A. L.; Yoon, S. S. Facile Processes for Producing Robust, Transparent, Conductive Platinum Nanofiber Mats. *Nanoscale* **2017**, *9*, 6076−6084.
(54) An, S.; Jo, H. S.; Kim, Y. I.; Song, K. Y.; Kim, M.-W.; Lee, K. B.; Yarin, A. L.; Yoon, S. S. Bio-Inspired, Colorful, Flexible, Defrostable Light-Scattering Hybrid Films for the Effective Distribution of Led Light. *Nanoscale* **2017**, *9*, 9139−9147.
(55) Kim, M.-W.; Yoon, H.; Ohm, T. Y.; Jo, H. S.; An, S.; Choi, S. K.; Park, H.; Al-Deyab, S. S.; Min, B. K.; Swihart, M. T. Nanotextured

https://dx.doi.org/10.1021/acsami.0c01697
ACS Appl. Mater. Interfaces XXXX, XXX, XXX−XXX

Cupric Oxide Nanofibers Coated with Atomic Layer Deposited Zno-TiO_2 as Highly Efficient Photocathodes. *Appl. Catal., B* **2017**, *201*, 479−485.
(56) Jo, H. S.; An, S.; Lee, J.-G.; Park, H. G.; Al-Deyab, S. S.; Yarin, A. L.; Yoon, S. S. Highly Flexible, Stretchable, Patternable, Transparent Copper Fiber Heater on a Complex 3d Surface. *NPG Asia Mater.* **2017**, *9*, No. e347.
(57) Kim, M.-W.; An, S.; Kim, K.; Kim, T.-G.; Jo, H. S.; Park, D.-H.; Yoon, S. S.; Yarin, A. L. Packing of Metalized Polymer Nanofibers for Aneurysm Embolization. *Nanoscale* **2018**, *10*, 6589−6601.
(58) Jo, H. S.; Kwon, H.-J.; Kim, T.-G.; Park, C.-W.; An, S.; Yarin, A. L.; Yoon, S. S. Wearable Transparent Thermal Sensors and Heaters Based on Metal-Plated Fibers and Nanowires. *Nanoscale* **2018**, *10*, 19825−19834.
(59) An, S.; Kim, Y. I.; Jo, H. S.; Kim, M.-W.; Swihart, M. T.; Yarin, A. L.; Yoon, S. S. Oxidation-Resistant Metallized Nanofibers as Ttransparent Conducting Films and Heaters. *Acta Mater.* **2018**, *143*, 174−180.
(60) Kim, Y. I.; An, S.; Kim, M.-W.; Jo, H.-S.; Kim, T.-G.; Swihart, M. T.; Yarin, A. L.; Yoon, S. S. Highly Transparent, Conducting, Body-Attachable Metallized Fibers as a Flexible and Stretchable Film. *J. Alloys Compd.* **2019**, *790*, 1127−1136.
(61) Kim, M.-W.; An, S.; Seok, H.; Jung, H.; Park, D.-H.; Yarin, A. L.; Yoon, S. S. In Vitro Evaluation of Pt-Coated Electrospun Nanofibers for Endovascular Coil Embolization. *Acta Biomater.* **2020**, 285−292.
(62) Jo, H. S.; An, S.; Park, C.-W.; Woo, D.-Y.; Yarin, A. L.; Yoon, S. S. Wearable, Stretchable, Transparent All-in-One Soft Sensor Formed from Supersonically Sprayed Silver Nanowires. *ACS Appl. Mater. Interfaces* **2019**, *11*, 40232−40242.
(63) Hernandez-Sierra, A.; Alguacil, F. J.; Alonso, M. Unipolar Charging of Nanometer Aerosol Particles in a Corona Ionizer. *J. Aerosol Sci.* **2003**, *34*, 733−745.
(64) Chen, G.; Xiao, H.; Wang, X. In *Study on Parameter Optimization of Corona Charging for Melt-Blown Polypropylene Electret Nonwoven Web Used as Air Filter*, IEEE 9th International Conference on the Properties and Applications of Dielectric Materials; IEEE: Harbin, China, 2009; pp 389−391.
(65) Lundgren, D. A.; Whitby, K. Effect of Particle Electrostatic Charge on Filtration by Fibrous Filters. *Ind. Eng. Chem. Process Des. Dev.* **1965**, *4*, 345−349.
(66) Liao, Z.; Li, Y.; Xiao, X.; Wang, C.; Cao, S.; Yang, Y. Electrostatic Precipitation of Submicron Particles with an Enhanced Unipolar Pre-Charger. *Aerosol Air Qual. Res.* **2018**, *18*, 1141−1147.
(67) Zhang, J.; Adamiak, K. A Multi-Species Dc Stationary Model for Negative Corona Discharge in Oxygen; Point-Plane Configuration. *J. Electrost.* **2007**, *65*, 459−464.
(68) Palm, P.; Adamovich, I.; Rich, J.; Ploenjes, E. In *Mitigation of Electron Attachment and Recombination in Atmospheric Pressure Air Plasmas*, 33rd Plasmadynamics and Lasers Conference, 2002; p 2224.
(69) Pontiga, F.; Soria, C.; Castellanos, A.; Skalny, J. D. A Study of Ozone Generation by Negative Corona Discharge through Different Plasma Chemistry Models. *Ozone: Sci. Eng.* **2002**, *24*, 447−462.

https://dx.doi.org/10.1021/acsami.0c01697
ACS Appl. Mater. Interfaces XXXX, XXX, XXX−XXX